Lehrstuhl für Bildverarbeitung
Institute of Imaging & Computer Vision

Multispectral filter wheel cameras: modeling aberrations with filters in front of lens

Julie Klein and Til Aach
Institute of Imaging and Computer Vision
RWTH Aachen University, 52056 Aachen, Germany
tel: +49 241 80 27860, fax: +49 241 80 22200
web: www.lfb.rwth-aachen.de

in: IS&T/SPIE Electronic Imaging: Digital Photography VIII. See also BibTeX entry below.

BibTeX:

```
@inproceedings{Klein2012,
  author = {Julie Klein and Til Aach},
  title = {Multispectral filter wheel cameras: modeling aberrations with filters in front of lens},
  booktitle = {{IS\&T/SPIE} Electronic Imaging: Digital Photography {VIII}},
  year = {2012},
  pages = {to appear},
  address = {San Francisco, CA, USA},
  month = {January 22--26},
  publisher = {SPIE},
  volume = {8299}
}
```


document created on: November 15, 2011
created from file: Klein2012.tex
cover page automatically created with CoverPage.sty
(available at your favourite CTAN mirror)

RWTH AACHEN
RHEINISCH-WESTFÄLISCHE TECHNISCHE HOCHSCHULE AACHEN

Multispectral filter wheel cameras: modeling aberrations for filters in front of lens

Julie Klein and Til Aach

Institute of Imaging and Computer Vision, RWTH Aachen University,
D-52056 Aachen, Germany

ABSTRACT

Aberrations occur in multispectral cameras featuring filter wheels because of color filters with different optical properties being present in the ray path. In order to ensure an exact compensation of these aberrations, a mathematical model of the distortions has to be developed and its parameters have to be calculated using the measured data. Such a model already exists for optical filters placed between the sensor and the lens, but not for bandpass filters placed in front of the lens. For this configuration, the rays are first distorted by the filters and then by the lens. In this paper, we derive a model for aberrations caused by filters placed in front of the lens in multispectral cameras. We compare this model with distortions obtained with simulations as well as with distortions measured during real multispectral acquisitions. In both cases, the difference between modeled and measured aberrations remains low, which corroborates the physical model. Multispectral acquisitions with filters placed between the sensor and the lens or in front of the lens are compared: the latter exhibit smaller distortions and the aberrations in both images can be compensated using the same algorithm.

Keywords: Multispectral camera, transversal aberrations, color filters, bandpass filters

1. INTRODUCTION

Multispectral cameras are used in many domains for accurate color reproduction, since by dividing the visible electromagnetic spectrum into more than three spectral channels they allow fulfilling the Luther rule[1] much better than common RGB cameras. One particular type of multispectral cameras features a monochrome sensor and five to thirteen optical bandpass filters.[2–12] The filters are positioned either between the lens and the sensor[2–4, 8, 13] or in front of the lens,[11] as shown in Fig. 1; these configurations will be referred to as configuration B and configuration F, respectively.

The configuration B is often preferred, for instance because filters placed in front of the lens must be bigger (and are thus more expensive) in order to avoid any vignetting effect. While the aberrations have already been modeled for this configuration,[2–4] no comparable model has been calculated for configuration F as far as the authors know. In this paper, a mathematical model is established for configuration F and parallels with the aberrations and model for configuration B are drawn.

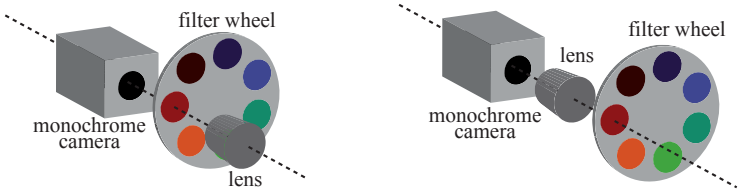

(a) (b)

Figure 1: Two possible positions for the filters: configuration B between the sensor and the lens (a) or configuration F in front of the lens (b). The aberrations modeled in this work concern configuration F.

Further author information:
Send correspondence to Julie Klein, E-mail: julie.klein@lfb.rwth-aachen.de, Telephone: +49 (0)241 80-27866

In the next section, we will expose the model for the transversal aberrations in configuration F and for the additional aberrations. We then give results obtained by simulating a camera with filters placed in front of the lens and measuring the aberrations. We also compare the aberrations in a real multispectral acquisition with the simulation and the model, before we finish with conclusions.

2. MODELING OF ABERRATIONS

The transversal aberrations appearing in the multispectral camera in configuration F are first caused by the color filter and then by the lens, as explained in the following paragraphs. Once these two types of distortions are modeled for an optical system featuring one given filter, it is possible to model the relative distortions between two different filters.

2.1 Filters aberrations

The calculation of the distortions caused by filters relies on the model depicted in Fig. 2. The objective is represented by a thin lens of focal length f and the filter is represented by a planar parallel plate of thickness l and refraction index n placed in front of the lens with a tilt angle φ. The tilt angle is practically small, but, due to unavoidable production spread of the filter wheel, it is not equal to zero, and varies from filter to filter. The ray that is considered has an angle θ with the optical axis and passes the center $\mathbf{O}$ of the lens when the filter is in the ray path. Without any filter, the image point of the considered object point is $\mathbf{X}$; the image point distorted because of the optical filter is $\mathbf{X}_f$.

To derive the filter aberrations $\mathbf{d}_s = \mathbf{X}_f - \mathbf{X}$ appearing on the sensor plane, the first step is the calculation of the distortion $\mathbf{d}_f$ caused by the filter and measured on the filter surface. Snell's law for the ray reaching the first filter surface states

$$\sin(\alpha) = n \ \sin(\beta) \tag{1}$$

with the angle α of the incoming ray relative to the filter normal, the angle β of the ray refracted by the first surface of the filter, the filter refraction index n and the refraction index of air set to 1. The distortion $\mathbf{d}_f$ can be measured using the points I, A and B and

$$\mathbf{d}_f = \vec{IB} - \vec{IA} \tag{2}$$

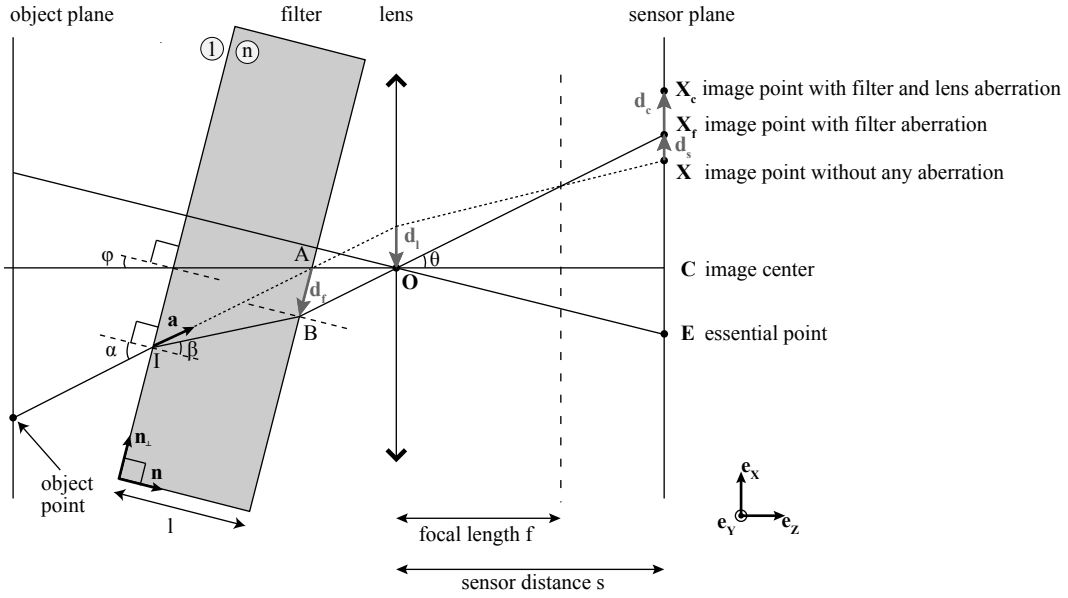

Figure 2: Model for the filters positioned in front of the lens.

The vector $\vec{IB}$ can be seen as a linear combination of the unit vector $\mathbf{a}$ defining the direction of the incoming ray and of the unit vector $\mathbf{n}$ which is perpendicular to the filter first surface

$$\vec{IB} = \xi_1 \ \mathbf{a} + \xi_2 \ \mathbf{n} \tag{3}$$

The two unknown coefficients ξ_1 and ξ_2 can be calculated using the projections of $\vec{IB}$ onto the two unit vectors $\mathbf{n}_\perp$ defining the filter first surface and $\mathbf{n}$ perpendicular to this surface, respectively

$$\begin{cases} \vec{IB} \cdot \mathbf{n}_\perp = \dfrac{l}{\cos(\beta)} \ \sin(\beta) = \xi_1 \ \sin(\alpha) \\ \vec{IB} \cdot \mathbf{n} = l = \xi_1 \ \cos(\alpha) + \xi_2 \end{cases} \tag{4}$$

where $\cdot$ represents the scalar product and l is the thickness of the filter. The values of the unknowns are then given by

$$\begin{cases} \xi_1 = \dfrac{l \ \sin(\beta)}{\cos(\beta) \ \sin(\alpha)} = \dfrac{l}{n \ \cos(\beta)} \\ \xi_2 = l - \xi_1 \ \cos(\alpha) = l \left(1 - \dfrac{\cos(\alpha)}{n \ \cos(\beta)}\right) \end{cases} \tag{5}$$

The vector $\vec{IA}$ is calculated using the intercept theorem

$$\frac{\vec{IA}}{l} = \frac{\mathbf{a}}{\cos(\alpha)} \tag{6}$$

Using Eq. (6) and Eq. (3) after insertion of Eq. (5), the equation giving the distortion $\mathbf{d}_f$ on the filter surface becomes

$$\begin{aligned} \mathbf{d}_f &= \frac{l}{n \ \cos(\beta)} \ \mathbf{a} + l \left(1 - \frac{\cos(\alpha)}{n \ \cos(\beta)}\right) \ \mathbf{n} - \frac{l}{\cos(\alpha)} \ \mathbf{a} \\ &= l \left(1 - \frac{\cos(\alpha)}{n \ \cos(\beta)}\right) \left(\mathbf{n} - \frac{1}{\cos(\alpha)} \ \mathbf{a}\right) \end{aligned} \tag{7}$$

Once the distortion $\mathbf{d}_f$ on the filter surface is known, the distortion $\mathbf{d}_l$ on the lens plane is defined as the sum of the distortion $\mathbf{d}_f$ and a vector having the same direction as $\mathbf{a}$

$$\mathbf{d}_l = \mathbf{d}_f + \xi_3 \ \mathbf{a} \tag{8}$$

The unknown coefficient ξ_3 can be calculated as previously using the projection of $\mathbf{d}_l$ onto the optical axis

$$\begin{aligned} \mathbf{d}_l \cdot \mathbf{e}_z &= 0 \\ &= l \left(1 - \frac{\cos(\alpha)}{n \ \cos(\beta)}\right) \left(\mathbf{n} \cdot \mathbf{e}_z - \frac{1}{\cos(\alpha)} \ \mathbf{a} \cdot \mathbf{e}_z\right) + \xi_3 \ \mathbf{a} \cdot \mathbf{e}_z \end{aligned} \tag{9}$$

thus yielding

$$\xi_3 = l \left(1 - \frac{\cos(\alpha)}{n \ \cos(\beta)}\right) \left(\frac{1}{\cos(\alpha)} - \frac{\mathbf{n} \cdot \mathbf{e}_z}{\mathbf{a} \cdot \mathbf{e}_z)}\right) \tag{10}$$

By inserting Eqs. (7) and (9) into Eq. (8), the distortion in the lens plane can be calculated using

$$\mathbf{d}_l = l \left(1 - \frac{\cos(\alpha)}{n \ \cos(\beta)}\right) \left(\mathbf{n} - \frac{\mathbf{n} \cdot \mathbf{e}_z}{\mathbf{a} \cdot \mathbf{e}_z} \ \mathbf{a}\right) \tag{11}$$

The distortion $\mathbf{d}_s$ along the sensor plane is then given by $\mathbf{d}_s = \frac{f-s}{s}\mathbf{d}_l$ with s the distance between the lens and the sensor and f the focal length of the lens:

$$\mathbf{d}_s = \frac{f-s}{s} \ l \left(1 - \frac{\cos(\alpha)}{n \ \cos(\beta)}\right) \left(\mathbf{n} - \frac{\mathbf{n} \cdot \mathbf{e}_z}{\mathbf{a} \cdot \mathbf{e}_z} \ \mathbf{a}\right) \ , \tag{12}$$

where the term $\frac{\mathbf{a}}{\mathbf{a}\cdot\mathbf{e}_z}$ can be actually replaced by $\frac{\mathbf{X}_f}{s}$ using the intercept theorem. To simplify the equations, we note $\kappa = \frac{f-s}{s}\ l\left(1 - \frac{\cos(\alpha)}{n\cos(\beta)}\right)$ and rewrite Eq. (12)

$$\mathbf{d}_s = \kappa\ \mathbf{n} - \kappa\ \frac{\mathbf{n}\cdot\mathbf{e}_z}{s}\ \mathbf{X}_f \tag{13}$$

which means that the distortion caused by the filter can be modeled by an affine transformation

$$\mathbf{d}_s = \begin{pmatrix} -\kappa\frac{\mathbf{n}\cdot\mathbf{e}_z}{s} & 0 & 0 & \kappa\ \mathbf{n}\cdot\mathbf{e}_x \\ 0 & -\kappa\frac{\mathbf{n}\cdot\mathbf{e}_z}{s} & 0 & \kappa\ \mathbf{n}\cdot\mathbf{e}_y \\ 0 & 0 & -\kappa\frac{\mathbf{n}\cdot\mathbf{e}_z}{s} & \kappa\ \mathbf{n}\cdot\mathbf{e}_z \end{pmatrix} \begin{pmatrix} \mathbf{X}_f \\ 1 \end{pmatrix} \tag{14}$$

The distortion term along the optical axis $\mathbf{e}_z$ is 0 since $\mathbf{X}_f = (x_f, y_f, s)^T$ and Eq. (14) can be simplified to

$$\mathbf{d}_s = \begin{pmatrix} -\kappa\frac{\mathbf{n}\cdot\mathbf{e}_z}{s} & 0 & \kappa\ \mathbf{n}\cdot\mathbf{e}_x \\ 0 & -\kappa\frac{\mathbf{n}\cdot\mathbf{e}_z}{s} & \kappa\ \mathbf{n}\cdot\mathbf{e}_y \\ 0 & 0 & 0 \end{pmatrix} \begin{pmatrix} x_f \\ y_f \\ 1 \end{pmatrix} = \mathbf{M}_f \begin{pmatrix} x_f \\ y_f \\ 1 \end{pmatrix} \tag{15}$$

with the matrix $\mathbf{M}_f \in \mathbb{R}^{3\times3}$.

For an object placed at infinite distance, the sensor plane coincides with the focus plane, i.e., $s = f$, and the distortion $\mathbf{d}_s$ thus becomes null. The rays coming from an object at infinite distance are parallel when no color filter is in their path and they focus on one given position in the focus plane. When a color filter is utilized, the rays are refracted twice at the surfaces of the filter but remain parallel and with the same direction at the output of the filter: they then focus exactly on the same position in the focus plane.

2.2 Relative filter distortions

We now consider the relative distortion $\mathbf{\Delta d}_s$ due to the insertion of a new filter in the ray path, i.e., the distortion caused when a filter F1 with the parameters l_1, n_1, φ_1, $\mathbf{n}_1$ (and consequently related to the angles α_1 and β_1) is replaced by a filter F2 with the parameters l_2, n_2, φ_2, $\mathbf{n}_2$ (and consequently related to the angles α_2 and β_2). Of course, the ray leaving the filter F2 does not necessarily pass through $\mathbf{O}$. The distortions on the sensor plane for these two filters are

$$\begin{cases} \mathbf{d}_{s,1} = \kappa_1\ \mathbf{n}_1 - \kappa_1\ \dfrac{\mathbf{n}_1\cdot\mathbf{e}_z}{s}\ \mathbf{X}_{f,1} \\ \mathbf{d}_{s,2} = \kappa_2\ \mathbf{n}_2 - \kappa_2\ \dfrac{\mathbf{n}_2\cdot\mathbf{e}_z}{s}\ \mathbf{X}_{f,1} \end{cases} \tag{16}$$

where $\kappa_i = \frac{f-s}{s}\ l_i\left(1 - \frac{\cos(\alpha_i)}{n_i\cos(\beta_i)}\right)$ for $i = 1, 2$. $\mathbf{X}_{f,1}$ is used in both equations because we replaced $\frac{\mathbf{a}}{\mathbf{a}\cdot\mathbf{e}_z}$ by $\frac{\mathbf{X}_{f,1}}{s}$. The relative distortion $\mathbf{\Delta d}_s = \mathbf{d}_{s,2} - \mathbf{d}_{s,1}$ is then given by

$$\mathbf{\Delta d}_s = \underbrace{\kappa_2\ \mathbf{n}_2 - \kappa_1\ \mathbf{n}_1}_{T1} - \underbrace{(\kappa_2\ \mathbf{n}_2\cdot\mathbf{e}_z - \kappa_1\ \mathbf{n}_1\cdot\mathbf{e}_z)\ \frac{\mathbf{X}_{f,1}}{s}}_{T2(\mathbf{X}_{f,1})}\ . \tag{17}$$

The first part of Eq. (17), $T1$, describes a global translation for all the image positions. and the second part of this equation, $T2(\mathbf{X}_{f,1})$, is an affine displacement that depends on the position $\mathbf{X}_{f,1}$ of the image point distorted by the filter F1. The relative filter distortion for the position $\mathbf{X}_{f,1} = (x_{f,1}, y_{f,1}, s)^T$ can thus be modeled by an affine transformation with the matrix $\mathbf{M}_f^{rel} \in \mathbb{R}^{3\times3}$

$$\mathbf{\Delta d}_s = \mathbf{M}_f^{rel} \begin{pmatrix} x_{f,1} \\ y_{f,1} \\ 1 \end{pmatrix} \tag{18}$$

The third row of the matrix $\mathbf{M}_f^{rel}$ is composed of 0 because the relative distortion is in the sensor plane, as in Eq. (15).

The position $\mathbf{X}_{f,2} = \mathbf{X}_{f,1} + \mathbf{\Delta d}_s$ of the image point distorted by the filter F2 thus is an affine transformation of the image point distorted by the filter F1. This result is comparable to the model of aberrations for filters placed between the lens and the sensor developed by Brauers et al.[2,3]

2.3 Lens aberrations

After the filter aberrations, the rays are also distorted by the lens. The lens distortions include the primary monochromatic aberrations and the chromatic aberrations.[14] These distortions are functions of the ray coordinates at the system aperture. The primary monochromatic aberrations are not affine but rather third-order terms.[15] In the case of paraxial imaging like in our optical system, the monochromatic aberrations are neglected and only the chromatic aberrations are taken into account. In this work, they are approximated by an affine model. The image points $\mathbf{X}_{f,1}$ and $\mathbf{X}_{f,2}$ are distorted to the image points $\mathbf{X}_{c,1}$ and $\mathbf{X}_{c,2}$, respectively, because of the lens aberrations. The distortions due to the lens are $\mathbf{d}_{c,1} = \mathbf{X}_{c,1} - \mathbf{X}_{f,1}$ and $\mathbf{d}_{c,2} = \mathbf{X}_{c,2} - \mathbf{X}_{f,2}$. They are calculated with an affine model using the matrices $\mathbf{M}_{c,1} \in \mathbb{R}^{3\times3}$ and $\mathbf{M}_{c,2} \in \mathbb{R}^{3\times3}$ according to

$$\begin{cases} \mathbf{d}_{c,1} = \mathbf{M}_{c,1} \begin{pmatrix} x_{f,1} \\ y_{f,1} \\ 1 \end{pmatrix} \\ \mathbf{d}_{c,2} = \mathbf{M}_{c,2} \begin{pmatrix} x_{f,2} \\ y_{f,2} \\ 1 \end{pmatrix} \end{cases} \tag{19}$$

We now seek to find the relative distortion between the two image points $\mathbf{X}_{c,1}$ and $\mathbf{X}_{c,2}$, which are the only image points we have access to in our images

$$\begin{aligned} \mathbf{X}_{c,2} - \mathbf{X}_{c,1} &= (\mathbf{X}_{c,2} - \mathbf{X}_{f,2}) - (\mathbf{X}_{c,1} - \mathbf{X}_{f,1}) + (\mathbf{X}_{f,2} - \mathbf{X}_{f,1}) \\ &= \mathbf{d}_{c,2} - \mathbf{d}_{c,1} + \boldsymbol{\Delta}\mathbf{d}_s \end{aligned} \tag{20}$$

From Eq. (18) and (19), we know that $\mathbf{d}_{c,1}$ and $\boldsymbol{\Delta}\mathbf{d}_s$ are affine functions of the image point $\mathbf{X}_{f,1}$. $\mathbf{d}_{c,2}$ is an affine function of the image point $\mathbf{X}_{f,2}$, which is in turn an affine function of the image point $\mathbf{X}_{f,1}$ according to Eq. (18) and $\mathbf{X}_{f,2} = \mathbf{X}_{f,1} - \mathbf{d}_{s,1} + \mathbf{d}_{s,2}$. This means that $\mathbf{X}_{c,2} - \mathbf{X}_{c,1}$ is an affine function of the image point $\mathbf{X}_{f,1}$, and thus also an affine function of the image point $\mathbf{X}_{c,1}$.

The whole distortion $\boldsymbol{\Delta}\mathbf{X}_c = \mathbf{X}_{c,2} - \mathbf{X}_{c,1}$ that we can measure on our images or our simulation is finally an affine function of the image point $\mathbf{X}_{c,1} = (x_{c,1}, y_{c,1}, s)^T$ that can be expressed as

$$\boldsymbol{\Delta}\mathbf{X}_c = \mathbf{M} \begin{pmatrix} x_{c,1} \\ y_{c,1} \\ 1 \end{pmatrix} \tag{21}$$

with the matrix $\mathbf{M} \in \mathbb{R}^{3\times3}$.

3. MEASUREMENTS OF ABERRATIONS

To evaluate the accuracy of the affine model we derived, we performed distortion measurements in optical systems featuring a color filter placed in front of a lens, utilizing simulation data as well as data acquired with a real imaging system.

We simulated the lens according to the data in [16] with the simulation software Zemax (Zemax Development Corporation, Bellevue, WA, USA) and measured the relative aberrations caused by two different color filters. The two filters had the same thickness, i.e., $l_1 = l_2$, and the same refraction index, i.e., $n_1 = n_2$, but different tilt angles: the reference filter was tilted by $+1^\circ$ around $\mathbf{e}_x$ and the filter for which the distortions were simulated by -1° around $\mathbf{e}_y$. The object imaged by this simulated optical system was a grid of 11×11 points. We compared the position on the sensor plane of these 121 object points distorted by the two filters. For each filter, we considered only rays from one given wavelength out of the 7 central wavelengths of the color filters of our real system.

Besides the simulation of a multispectral camera, we also acquired real multispectral images to measure the distortions with this real optical system. The 7 color filters we utilize have central wavelengths going from 400 nm to 700 nm in steps of 50 nm and bandwidths of about 40 nm and are mounted in a motorized filter wheel. The

lens is an aspherical AF-S DX Nikkor 18-70 nm, which is similar to the lens used for the simulation, and the monochrome camera is a IDS uEye 2240 CCD camera. In this case, the distortions were not measured using some points of interest spread over the image like for the simulation. Instead, we divide the image into 90 regions of interest and calculate for each of these the displacement due to the current filter relative to the reference filter using mutual information as similarity measure. This results in a field of displacement vectors as shown in Fig. 4. The "random sample consensus" (RANSAC) algorithm is then utilized to remove stochastic errors in the vector field. More details about this measurement are provided by Brauers et al.[3]

We also directly compared two multispectral images acquired with the two configurations shown in Fig. 1. We used the same monochrome camera, filter wheel and lens to perform the two acquisitions.

4. RESULTS

The aberrations of configuration F measured with the simulated optical system are shown in Fig. 3a. For these results, we utilized as reference color filter the filter with wavelength 700 nm, that is, we traced the rays only for the wavelength 700 nm, and measured the distortions for the color filter with wavelength 500 nm. The object points that were followed are the corners of a grid. The simulated distortions and the results of our model are shown in the figure with black and white vectors, respectively. At the corners of the sensor plane, the distortions are about 2.8 pixels. The vectors of the simulated and of the modeled relative distortions are very close and the errors are below 0.047 pixel (see Fig. 3b): this indicates that the affine model is well suited for multispectral cameras with optical filters placed in front of the lens.

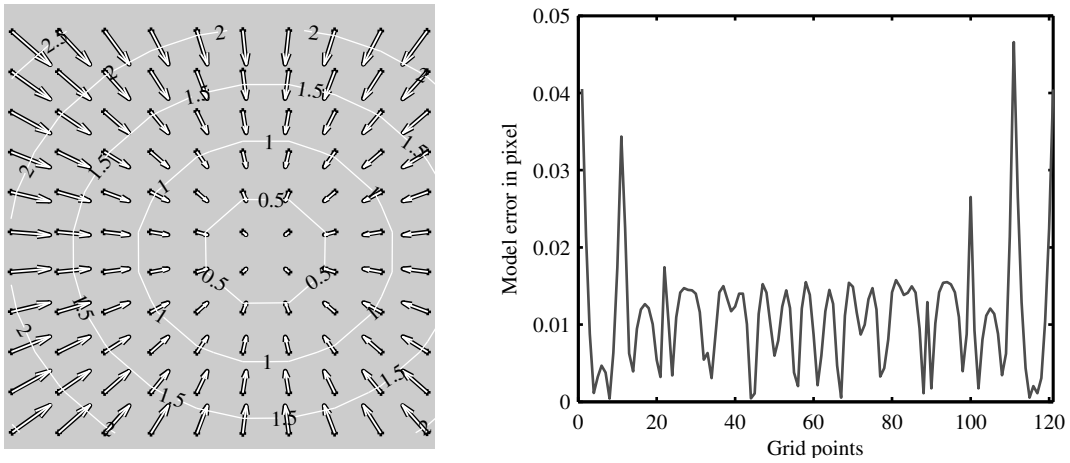

(a) (b)

Figure 3: Aberrations simulated for the corner positions of a grid for the color channel 500 nm relative to the color channel 700 nm (black vectors) and distortions calculated with our model (white) (a). The isolines correspond to the lengths of the modeled distortions, in pixels. The pixel errors between the simulated and the modeled distortions are shown in (b) for the 121 grid points.

We also compared the image points simulated for the filter with wavelength 450 nm to the image points for the 6 other filters. The reference filter was tilted by $+1^\circ$ around $\mathbf{e}_x$ and the other filters by -1° around $\mathbf{e}_y$. The mean and maximum errors of our model are summarized in Tab. 1 for all filters: the mean errors lie mostly below 0.01 pixel and the maximum error is 0.0522 pixel. These low errors corroborate our affine model.

For the real acquisition data, we did not used points of interest in the image to measure the distortions, but rather whole regions, as explained in Sec. 3. As can be seen in Fig. 4a, the aberrations measured on separate blocks of the image (black vectors) and the aberrations from the affine model (white vectors) are very close. Outliers are possible during the measurement of the distortions (see the black vector on the bottom of the image) and are eliminated using the RANSAC algorithm. The distortions measured between the color channels 650 nm and 550 nm are larger than the simulated ones, reaching 8 pixels instead of 2.8 pixels for the simulation.

Error	Filter						
(in pixel)	400 nm	450 nm	500 nm	550 nm	600 nm	650 nm	700 nm
Maximum	0.0522	0.0342	0.0189	0	0.0168	0.0259	0.0337
Mean	0.0131	0.0080	0.0039	0	0.0034	0.0057	0.0077

Table 1: Maximum and mean values of the model errors for the seven filters based on simulated data. The reference filter here is filter 550 nm and the values are calculated over the 121 grid points.

This can be explained by the filter parameters: the tilt angles were set to $\pm 1°$ for the simulation, but the real values are almost certainly different. The thickness and refraction index of the real filters may also be not exactly the same as in the simulation. The errors of the model plotted in Fig. 4b are only calculated for the regions marked as inliers by the algorithm. They are higher than with the simulation data: the mean error for this filter is 0.2098 pixel. The mean and maximum errors for the other filters can also be taken from Tab. 2. The errors are 10 to 100 times higher than the errors in the simulation data, but remain low with mean errors of about 0.2 pixels for all the filters. This can be explained by the distortions themselves that are much larger than during the simulation. Another explanation can be the bandwidth of the filters we used: it is about 40 nm, whereas for the simulation we considered narrowband filters by taking only rays with the filters central wavelengths. This would mean that the model for the chromatic aberrations we used could be improved with one of the models explained by Klein et al.[17] for instance.

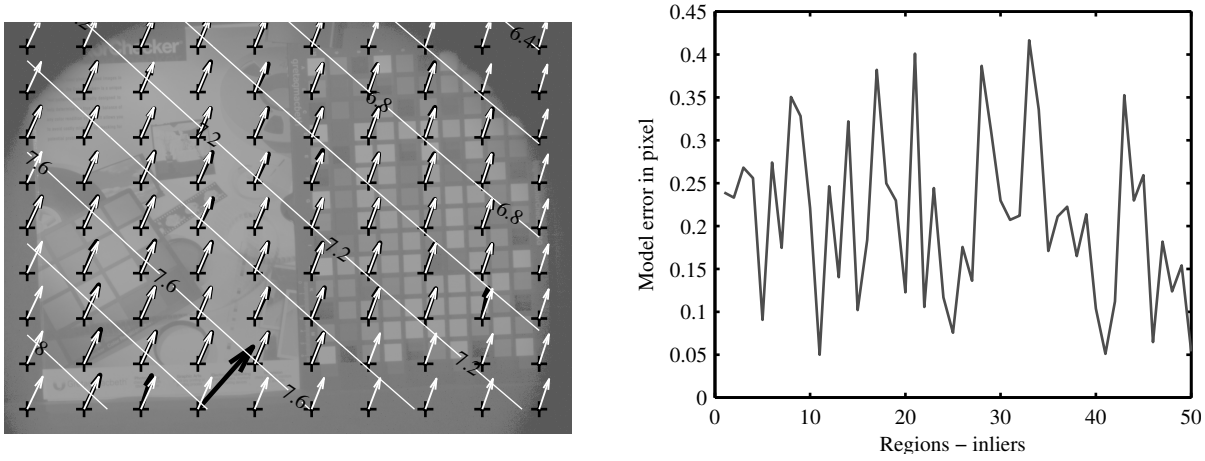

(a) (b)

Figure 4: Distortions measured for color channel 650 nm relative to color channel 550 nm (black vectors) and model values resulting from this measurement (white) (a). The vignetting effect is visible on the background image from color channel 650 nm. The pixel errors between the measured and the modeled distortions are shown in (b) for the 50 regions of interest that are not outliers of the RANSAC algorithm.

Error	Filter						
(in pixel)	400 nm	450 nm	500 nm	550 nm	600 nm	650 nm	700 nm
Maximum	0.5587	0.5097	0.3995	0	0.4652	0.4168	0.4120
Mean	0.2314	0.2108	0.1838	0	0.1901	0.2098	0.1961

Table 2: Maximum and mean values of the model errors for the seven filters based on real data. The reference filter here is filter 550 nm and the values are calculated over the inliers of the RANSAC algorithm.

The matrices for the affine model of the aberrations are very similar for the simulation and for the real data, as can be seen in Tab. 3. The last row terms are 0, since the aberrations are in the sensor plane, i.e., perpendicular to $\mathbf{e}_z$. The diagonal terms are close to 1, the amplitude of the translation terms (third column) and of the shear terms (terms at positions (1,2) and (2,1) in the matrix) are larger for the real image acquisition than for the simulation.

Simulation:

$$\mathbf{M} = \begin{pmatrix} 1.0025 & 0.0000 & -0.1749 \\ 0.0000 & 1.0025 & 0.1731 \\ 0 & 0 & 0 \end{pmatrix}$$

Real acquisition:

$$\mathbf{M} = \begin{pmatrix} 0.9989 & 0.0005 & 3.0588 \\ 0.0005 & 0.9992 & -6.5913 \\ 0 & 0 & 0 \end{pmatrix}$$

Table 3: Example matrices for the affine model of the system aberrations from Eq. (21) for our simulation and our acquisition of real images. The distortion matrix for the simulation corresponds to Fig. 3a and the distortion matrix for the real acquisition corresponds to Fig. 4a.

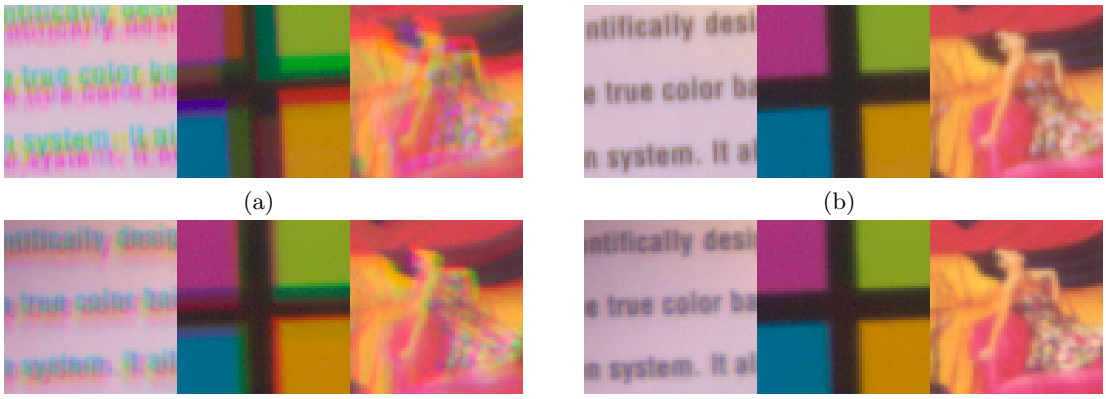

(a) (b) (c) (d)

Figure 5: Regions of a multispectral acquisition with configuration B (a) and with configuration F (c). The corresponding images with corrected aberrations are (b) and (d), respectively. Matrices for the corrections are given in Tab. 4. Each region represents an area of 61×61 pixels.

We also directly compared the distortions of two multispectral imaging systems in configuration B and configuration F. Parts of the resulting image are shown in Fig. 5. The images obtained with configuration F (Fig. 5c) are almost as much distorted as the images obtained with configuration B (Fig. 5a). The same algorithm[3] was utilized to compensate the distortions in the two filter configurations and the undistorted images in Figs. 5d and 5b do not exhibit any remaining distortion such as color fringes. This means that the algorithm that has been developed for configuration B[3] can also be used to capture and compensate the transversal aberrations for configuration F. Matrices of the affine model for the two configurations are compared in Tab. 4. The matrices for the real acquisitions in the two different configurations are much closer compared to the matrices for simulation and real data in Tab. 3. The amplitude of the translation terms and of the shear terms are comparable for the two configurations.

configuration B:

$$\mathbf{M} = \begin{pmatrix} 0.9997 & 0.0006 & 1.1593 \\ 0.0002 & 0.9997 & 5.7883 \\ 0 & 0 & 0 \end{pmatrix}$$

configuration F:

$$\mathbf{M} = \begin{pmatrix} 1.0000 & 0.0002 & 2.7455 \\ 0.0002 & 1.0000 & 1.2008 \\ 0 & 0 & 0 \end{pmatrix}$$

Table 4: Example matrices for the affine model of the system aberrations from Eq. (21) for configuration B and configuration F. The distortion matrix for configuration B corresponds to Fig. 5a and the distortion matrix for configuration F corresponds to Fig. 5c.

5. CONCLUSIONS

We have developed a model for the aberrations in multispectral cameras where the optical filters are placed in front of the lens. Assuming a perfect lens without aberrations, the distortions are affine and the model is similar to the one for cameras with filters positioned between the lens and the sensor. We have confirmed the model by both simulating multispectral imaging with optical filters in front of the lens and acquiring real image with such a camera. After compensation of the distortions using our affine model, no color fringes remain visible. The model could further be improved by considering another model for the lens aberrations.

6. ACKNOWLEDGMENTS

The authors acknowledge gratefully funding by the German Research Foundation (DFG, grant AA5/2–1).

REFERENCES

[1] Luther, R., "Aus dem Gebiet der Farbreizmetrik," *Zeitschrift für technische Physik* **8**, 540–558 (1927).

[2] Brauers, J., Schulte, N., and Aach, T., "Modeling and compensation of geometric distortions of multispectral cameras with optical bandpass filter wheels," in [*15th European Signal Processing Conference*], 1902–1906 (September 2007).

[3] Brauers, J., Schulte, N., and Aach, T., "Multispectral filter-wheel cameras: Geometric distortion model and compensation algorithms," *IEEE Transactions on Image Processing* **17**, 2368–2380 (December 2008).

[4] Brauers, J. and Aach, T., "Geometric calibration of lens and filter distortions for multispectral filter-wheel cameras," *IEEE Transactions on Image Processing* **20**, 496–505 (February 2011).

[5] Burns, P. D. and Berns, R. S., "Analysis multispectral image capture," in [*Proc. IS&T/SID 4th Color Imaging Conference (CIC)*], **4**, 19–22 (November 1996).

[6] Haneishi, H., Iwanami, T., Honma, T., Tsumura, N., and Miyake, Y., "Goniospectral imaging of three-dimensional objects," *Journal of Imaging Science and Technology* **45**(5), 451–456 (2001).

[7] Helling, S., Seidel, E., and Biehlig, W., "Algorithms for spectral color stimulus reconstruction with a seven-channel multispectral camera," in [*Proc. IS&Ts 2nd European Conference on Color in Graphics, Imaging, and Vision (CGIV)*], **2**, 254–258 (April 2004).

[8] Imai, F. H., Quan, S., Rosen, M. R., and Berns, R. S., "Digital camera filter design for colorimetric and spectral accuracy," in [*Proceedings of the Third International Conference on Multispectral Color Science, IS&T*], 13–16 (June 2001).

[9] Mansouri, A., Marzani, F. S., Hardeberg, J. Y., and Gouton, P., "Optical calibration of a multispectral imaging system based on interference filters," *SPIE Optical Engineering* **44**, 027004.1–027004.12 (February 2005).

[10] Ribés, A., Schmitt, F., Pillay, R., and Lahanier, C., "Calibration and spectral reconstruction for CRISATEL: An art painting multispectral acquisition system," *Journal of Imaging Science and Technology* **49**, 563–573 (November/December 2005).

[11] Tominaga, S., Fukuda, T., and Kimachi, A., "A high-resolution imaging system for omnidirectional illuminant estimation," *Journal of Imaging Science and Technology* **52**, 040907–1 – 040907–9 (July/August 2008).

[12] Vilaseca, M., Mercadal, R., Pujol, J., Arjona, M., de Lasarte, M., Huertas, R., Melgosa, M., and Imai, F. H., "Characterization of the human iris spectral reflectance with a multispectral imaging system," *Applied Optics* **47**, 5622–5630 (October 2008).

[13] Hardeberg, J. Y., "Recent advances in acquisition and reproduction of multispectral images," in [*EURASIP 14th European Signal Processing Conference*], (2006).

[14] Gross, H., Zügge, H., Peschka, M., and Blechinger, F., [*Handbook of Optical Systems*], vol. 3: Aberration Theory and Correction of Optical Systems, Wiley VCH Verlag GmbH (2007).

[15] Smith, W. J., [*Modern Optical Engineering*], McGraw-Hill (2000).

[16] Hayakawa, S., "Zoom lens system." Patent (March 2005). US. Pat. 2005/0068636 A1.

[17] Klein, J., Brauers, J., and Aach, T., "Spatio-spectral modeling and compensation of transversal chromatic aberrations in multispectral imaging," *Journal of Imaging Science and Technology* (2011). Accepted for publication.